Chapter 5: Production of Tyrosine Kinase Inhibitors from *Streptomyces fragilis*

5.1 Introduction

Fermentation strategies employing *Streptomyces* species are prominent modalities for synthesizing indispensable medicinal therapeutics and their precursor compounds. The extraction of bioactive compounds from the complex fermentation broth is a critical step, and various extraction methodologies are utilized depending on the nature of the compounds being targeted. Common techniques include solid-liquid extraction, liquid-liquid extraction, and supercritical fluid extraction (Hewitt & Nienow, 2007; Ser et al., n.d.; Teke et al., 2022).

Streptomyces belongs to the largest genus of the phylum Actinobacteria, whose GC content of genetic material is rich with 70% coverage (Chandra & Chater, 2014). They possess the capability to produce secondary metabolites such as anticancer agents, immunosuppressive agents, and antibiotics. Genus *Streptomyces* plays a pivotal role in the field of drug discovery, contributing to a staggering 80% of the antibiotics developed today (de Lima Júnior et al., 2023)**.** Apart from antibiotics, *Streptomyces* bacteria also produce a wide array of complex secondary metabolites, including caspase-3 activators, protein kinase inhibitors, and apoptosis inducers, which have shown promising efficacy in cancer treatment. For instance, the anticancer drug bleomycin, synthesized by *Streptomyces verticillus***,** gained FDA approval in 1973 and is therapeutically effective in treating head and neck cancer, testicular cancer, cervical cancer, and lymphoma (Q. Gao et al., 2022). One of the anticancer drugs produced by *Streptomyces* species is the anthracycline group, which includes doxorubicin and daunorubicin (Shrestha et al., 2019).

Streptomyces fragilis is a soil bacteria that belong to the phylum Actinobacteria. It produces the tumor-inhibiting antibiotic Azaserine, which targets nucleic acid and demonstrates efficacy against gram-positive and gram-negative bacteria, protozoa, and fungi (Pittillo & Hunt, 1967; Van Cura et al., 2023). It also produces the enzyme α-amylase. This strain produces several secondary metabolites through fermentation, such as kinase and phosphatase inhibitors, which can be lead molecules in target-based cancer treatment (Law et al., 2019).

In this chapter, a focus is made on isolating and characterizing a strain that significantly resembles Streptomyces fragilis (NRRL2424), from sheep wool, and submerged fermentation was employed to produce protein kinase inhibitors (PKIs). Using *Streptomyces 85E* as a model, various crude extracts from different media were examined to ascertain the presence of PKIs.

This chapter also focused to explore the eukaryotic protein kinase inhibitory potential and anticancer efficacy of *Streptomyces fragilis* on human breast cancer, Lung cancer, cervical cancer and prostate cancer. Additionally, the free radical scavenging activity of extracts was elucidated through the DPPH assay. DPPH (2,2-diphenyl-1-picrylhydrazyl) is a stable free radical that measures free radical scavenging activity. Antioxidant compounds interact and provide hydrogen atoms to the DPPH, converting it into 2,2-diphenyl-1-picrylhydrazine (DPPH) (R. Singh et al., 2007). The free radicals are implicated in the auto-oxidation of unsaturated lipids present in food. Antioxidant molecules intervene in this oxidative chain reaction by donating hydrogen atoms derived from phenolic hydroxyl groups and creating a stable end product, effectively inhibiting further lipid oxidation (Ajila et al., 2007; Naidu et al., 2008).

Furthermore, the inhibitory potential of bioactive compounds from *Streptomyces fragilis* against various receptor tyrosine kinases, including VEGFR, CDK4, BCR-ABL, JAK2,

BCL2, and EGFR, was investigated. Receptor tyrosine kinases play a crucial role in controlling cellular signaling processes such as metabolism, differentiation, and cell proliferation. Mutations or overexpression of these protein kinases can lead to the development of various cancers. By targeting these enzymes, the bioactive compounds from *Streptomyces fragilis* may offer promising therapeutic strategies for cancer treatment, highlighting their significance in the development of new anticancer drugs.

5.2 Materials and methods

5.2.1 Isolation and maintenance of Actinomycetes

A wool sample for microbial isolation was obtained from sheep at the Veterinary Department of Banaras Hindu University utilizing sterile polyethylene packaging. The sample, consisting of 1 gram of wool, was mixed with 10 mL of distilled water at room temperature and homogenized via vortexing. Subsequently, the sample was subjected to serial dilution followed by the spread plate method, isolating individual colonies for further analysis. The isolated colonies were subsequently streaked to identify and isolate *Streptomyces sp.* for the present study. These strains were maintained on ISP4-Agar media, which consisted of (w/v) ammonium sulfate (0.2%), di-potassium hydrogen phosphate (0.1%), magnesium sulfate (0.1%), sodium chloride (0.1%), calcium carbonate (0.2%), soluble starch (1.0%), agar (2%), and Trace Salt Solution (TSS) [ferrous sulfate (0.1%), zinc sulfate (0.2%), copper sulfate (0.7%), and manganous chloride (0.8%)], with an initial pH adjusted to 7.0. The isolated and marker strains were sub-cultured monthly to ensure proper growth maintenance on ISP-4 agar media plates (Kobayashi et al., 1994).

5.2.2 Cultural and Morphological Properties

The isolated actinomycete was subjected to cultural and morphological assessments based on its growth pattern and colony morphology. The presence of spore-containing hyphae and aerial or substrate mycelium in the actinomycetes were carefully examined. Moreover, the properties of the actinomycete's cell wall were investigated using Gram

staining, utilizing a light microscope at 100x magnification (Al-Ansari et al., 2020; Khadayat et al., 2020).

5.2.3 16S rRNA Sequencing and Phylogenetic Analysis

16S rRNA sequencing was conducted for genetic analysis of genomes presented in the isolated actinomycete samples. It was scraped from the Petri plates and kept at -80°C before DNA extraction. A spin column kit of Hi-Media manufacturer was used for chromosomal DNA extraction, which further undergoes PCR (polymerase chain reaction) in a thermal cycler for bacterial 16S rRNA gene (1500 bp) amplification and then purified using Exonuclease 1- Shrimp Alkaline Phosphatase (Exo-SAP) (Clarridge III, 2004; Darby et al., 2005). Universal primers 530F and 800R were used for sequencing. Using the Sanger method, the 3500xL genetic analyzer (Life Technologies, USA) was incorporated to sequence purified genes. Obtained sequence files were edited using CHROMASLITE (version 1.5) and further analyzed using BLAST (Basic Local Alignment Search Tool) to search and get its closest similar sequence from NCBI (National Centre for Biotechnology Information (Altschul et al., 1990). Further multiple sequence alignment and phylogenetic analysis were performed for reliable species prediction and evolutionary interaction (Karlin & Altschul, 1990; Myers & Miller, 1988). Mega X performed multiple sequence alignments and constructed Neighbor-Joining phylogenetic trees. The stability of relationships was evaluated by a Bootstrap analysis of 1,000 trials (Kokkinos et al., 2010). The analyzed 16S rRNA sequence has been deposited in the NCBI GenBank database with the accession number **OL823085.**

5.2.4 Fermentation

5.2.4.1 Fermentation media: The media used for bioactive compound production were prepared in four different 500 mL flasks with 100 mL volume of four-broth media. The media and its content is specified as media-M:1 (Glycerol 3%, peptone 0.75%, glucose

0.3%, sodium chloride 0.3%, calcium carbonate 0.3%, yeast extract 0.2%, sodium nitrate 0.1%, and TSS), media-M:2(soluble starch 2%, glucose 1.5%, peptone 0.3%, yeast extract 0.2%, corn steep liquor 0.2%, sodium chloride 0.2%, calcium carbonate 0.2%, ammonium sulphate 0.05%, cobalt chloride 0.0001% and TSS, media-M:3 (Glucose 5%, yeast extract 1.1%, calcium carbonate 0.5%, peptone 0.4%, beef extract 0.4% and sodium chloride 0.25%) and media-M:4 (soluble starch 1%, glucose 1%, peptone 0.75%, malt extract 0.75%, sodium chloride 0.3%, magnesium sulphate 0.1% and TSS) and the seed media(glucose 1.5%, peptone 0.75%, yeast extract 0.75%, corn steep liquor 0.5%, sodium chloride 0.5% and calcium carbonate 0.2%). All the media were autoclaved properly prior to inoculation (Shanbhag et al., 2015b).

5.2.4.2 Fermentation condition: An inoculum was obtained via the use of a sterile loop to collect a sample from a 3-day-old culture plate, which was subsequently homogenized within 50 mL of seed medium and incubated for 72 hours under rotary agitation at a temperature of 30°C. The production media, consisting of media-M:1, media-M:2, media-M:3, and media-M:4, were sterilized through autoclaving prior to inoculation with 3 mL of inoculum obtained from the aforementioned seed culture. The inoculated flasks, containing a total volume of 100 mL of production media, were incubated under 200 rpm rotary agitation at 30°C for an additional 72 hours (Shanbhag et al., 2015b).

5.2.5 Production and Downstream Process of Secondary Metabolites

After the fermentation, a downstream process was carried out through a two-phase solvent extraction technique to recover the crude extract containing biosynthetic secondary metabolites (Madduri, Kennedy, Rivola, Inventi-Solari, Filippini, & Zanuso, G., ... & Hutchinson, 1998). The broth was split into two halves and processed as follows.

Aqueous extraction: Half of the broth was centrifuged at 6000 rpm for 20 minutes at 4°C. The supernatant was taken in a separate tube, and the cell debris in the little left-over

supernatant was sonicated for 30 minutes with a 10-minute cycle and 5 5-minute breaks. After sonication, it was again centrifuged to extract any intracellular product, and its supernatant was also taken out. The crude extracts were combined, lyophilized, and stored at -20°C.

Organic extraction: Another part of the broth was sonicated and mixed with twice its volume of chloroform: isopropanol (1:6 v/v) and incubated for 24 hours at 45±1°C and 200 rpm. After incubation, the organic part was collected from the broth by a conical separating funnel, followed by vacuum evaporation. The obtained crude extract was stored at -20°C.

5.2.6 Protein kinase inhibitory Assay (*Streptomyces 85E* assay)

The anticancer potential of the obtained extracts was elucidated through the protein kinase inhibitory assay. The extracts were thawed and mixed in DMSO at a 20 mg/mL concentration, sterilized using a sterile 0.45 µm nylon syringe filter, and the filtrate was stored at -20°C for instant use. *Streptomyces 85E* (ATCC 55824) strains are suitable for testing various kinase inhibitors using agar diffusion methods. Its growth and development are perfect on solid media and help identify the cytotoxicity of tested inhibitors. *Streptomyces 85E* strains were grown in LB broth media at 30 °C for three days at 180 rpm. This culture was later used to inoculate the plates of ISP-4 agar media through the spread plate method. A 6 mm well was created in these plates using a sterile cork borer, and a 160 µL sample was loaded. The plates were incubated for three days at 30 °C and later visualized for any sign of protein kinase inhibition activity (Watersa et al., 2002). Pure DMSO and doxorubicin (a well-known tyrosine kinase inhibitor) were utilized as the negative and positive controls, respectively.

5.2.7 Free radical scavenging activity

The free radical scavenging activity of organic and aqueous extracts of *Streptomyces fragilis* was elucidated through DPPH assay using the methodology outlined by Kamble et al., with minor changes (Kamble et al., 2018). The DPPH assay quantifies the ability of the extract or compounds to reduce the free radicals through a one-electron reduction process. Briefly, varying concentrations (1 to 40 µg/mL) of *Streptomyces fragilis* extract were prepared with a total volume of 3 mL in test tubes. In each test tube, 1 mL of a 0.1 mM DPPH solution was mixed and shaken vigorously. Subsequently, the test tubes were kept in the dark at room temperature for a duration of 30 minutes. A similar procedure was conducted with positive control L-ascorbic acid. To quantify the changes, the absorbance was taken at 517 nm a wavelength using spectrophotometry. The extent of radical scavenging activity was expressed as the percentage of inhibition and computed using the following formula:

$$\text{Inhibition percentage} = [(Ab_0 - Ab_s) \div Ab_0] \times 100$$

Where Ab_o is the absorbance of negative control, and Ab_s is the absorbance of the sample. The results were plotted against the sample concentration as the percentage of scavenging activity. The IC_{50} value was calculated from the graph, which is the concentration needed to achieve 50% free radical scavenging activity.

5.2.8 Cytotoxicity Activity by MTT Assay

The cytotoxic potential of the organic crude extract of *Streptomyces fragilis* was conducted against MCF-7 (Human breast cancer), Hop-62 (Lung cancer), SiHa (cervical cancer), and PC-3 (prostate cancer) cell lines through the MTT assay. All the cancer cell lines were cultivated in T-25 flasks, detached using trypsin, and collected in a 5 mL centrifuge tube. Subsequently, centrifugation was carried out at 300 x g to generate a cell pellet. The cell count was then adjusted using DMEM-HG medium to achieve approximately 10,000 cells suspended in 200 µL. Then, 200 µL of the cell suspension was

added to each well of a 96-well microtiter plate. The plate was then placed in an incubator at 37°C with 5% CO2 for 24 hours.

Following the incubation period, the used medium was extracted, and 200 µL of different concentrations of extracts (10 to 80 µg/mL) were introduced into their respective wells. The plate was subsequently placed in an incubator at 37°C with a 5% CO2 environment for 24 hours. After this, the medium containing the drug was discarded, and 200 µL of medium containing 10% MTT reagent was applied to each well, resulting in a final concentration of 0.5 mg/mL. Subsequently, the plate was incubated at 37°C with 5% CO2 for 3 hours. Following this period, the culture medium was removed without disrupting the crystals. In the next step, 100 µL of DMSO was added, and the plate was gently agitated using a gyratory shaker to dissolve the resultant formazan crystals. Absorbance readings were then obtained using a microplate reader at both 570 nm and 630 nm wavelengths. The percentage of growth inhibition was computed after subtracting the background and blank readings. From the dose-response curve, the concentration of crude extract required to inhibit 50% of cell growth (IC_{50}) was determined (Ren et al., 2016; Zhelyazkova et al., 2021).

5.2.9 Identification of secondary metabolites through HR-LCMS

The metabolites present in the extract samples were detected using the HR-LCMS technique (Holčapek et al., 2012). The required amount of dry sample was mixed in acetonitrile. It was analyzed using Thermo Fischer Scientific Q-Exactive Plus Biopharma-High Resolution Orbitrap Liquid Chromatograph Mass Spectrometer (HR-LCMS) connected with Hypersil GOLD C18 100 x 2.1 mm-3-micron column, HiP Sampler (model: G4226A), binary pump (model: G4220B), Column compartment (model: G1316C), and Diode-Array Detector (model: G4212B) of Agilent Technologies. The chromatography system was equilibrated with 5% Acetonitrile, and analysis was

done with 100% Acetonitrile at a flow rate of 0.3mL/min for 30 minutes by injecting a 5.00 µL sample volume. The Mass Spectrometer Q-ToF (model: G6550A) analysis was done for organics for aqueous extract with Sheath Gas Temperature (°C) 300, Nebulizer (psig) 35, Gas Flow (l/min) 13, and Gas Temp (°C) 250.

5.2.10 Molecular docking

Streptomyces 85E can show its non-aerial mycelia formation in the presence of any metabolite with any mode of inhibition. To get a brief knowledge of what metabolites could have hit on which receptor, an *Insilco* approach has been adapted. The compounds obtained from HR-LCMS were drawn using Marvin Sketch 21.12, ChemAxon (https://www.chemaxon.com), and saved in mol2 format. Different protein kinases structure were obtained from the PDB database (www.rcsb.org) like JAK2 (PDB: 4AGD), PDGFR (6JOI), EGFR (5ZWJ), PI3K (3L13), BCR-ABL (3QRJ) and BCL-2 (4AQ3) and CDK4 (Cdk4 with inhibitor not available, thus align cdk2 complex with cdk4, delete cdk2, ligand remained, then self-dock it) (Al-Warhi et al., 2020; Chan et al., 2011; Hanan et al., 2016; Ji et al., 2006; Kashima et al., 2020; M. McTigue et al., 2012; Nemaysh & Luthra, 2017; Perez et al., 2012; Zhao et al., 2018). The ligands were analyzed for their drug likeness and were calculated using Schrödinger's QikProp module (Schrödinger Release 2022-2). It incorporates Lipinski's rule of five, including the Logarithm of partition coefficient between n-octanol and water (miLogP), molecular weight (MWt), number of H-bond donors (nOHNH), number of H-bond acceptors (nOH) (Lipinski, 2004). The structure of proteins was optimized through the Protein Preparation Wizard of Schrodinger Suite. All the structural shortcomings were rectified using the EPIK module. All the water molecules were removed from the 0 Å distance of the ligand, and then the structure was minimized to its stable form using the OPLS4 Force field. The ligands were prepared using the LigPrep (Schrödinger Release 2022-2) module with an OPLS4 force

field, neutralizing ionization state, one structure for rapid screening, and the other with default settings. The receptor grid generator module generates each protein's grid along with the protein as receptor input for docking. The grid generation involved picking a co-crystalized ligand of the loaded protein and creating a grid box over the site. The docking of each protein was performed on the prepared ligand library using the Glide of the Schrodinger suite in Extra Precision mode (XP) with ten poses per ligand included during post-docking minimization. The result was analyzed with an Ascending Glide score.

5.2.11 Molecular Dynamics Simulation

Selected docked protein-ligand structures were taken into account for the molecular dynamics simulation run using the Desmond package containing the Schrödinger Suite. Counter ions neutralize the orthorhombic solvation system filled with TIP3 water model, and then the system was raised to 0.15 M NaCl concentration, followed by 1000 ps minimization. Then, the Molecular dynamics process in the OPLS_2005 force field was simulated for 200 ns with a trajectory recording interval of every 0.25 ns. MD was performed as a control for the standard ligands in all respective structures using the same protocol described above (Saini et al., 2023b).

The root mean square deviation (RMSD), root mean square fluctuation (RMSF), solvent accessible surface area (SASA), the radius of gyration (rGyr), and molecular interactions between protein and ligand complexes were calculated and examined after completion of the MD simulation. The binding free energy of complexes (MM-GBSA) was assessed using the following equation:

$$\Delta G_{binding} = \Delta G_{complex} - [\Delta G_{protein} + \Delta G_{ligand}]$$

Where $\Delta G_{binding}$ represents the binding free energy of the complexes, $\Delta G_{protein}$ and ΔG_{ligand} are energies of protein and ligand, respectively. For this purpose, the last 20 ns trajectories

were incorporated for MM-GBSA and per-residue decomposition calculation using the prime module (Kumari, Saini, Bhatnagar, et al., 2023).

5.3 Results and Discussion

5.3.1 Strain morphology and its identification

The isolated strain was characterized by its unique sporulation and formation of vegetative and aerial mycelium, as well as normal growth and abundant sporulation. The strain morphology and phylogenetic analysis of the isolated actinomycetes are represented in Figure 5.1.

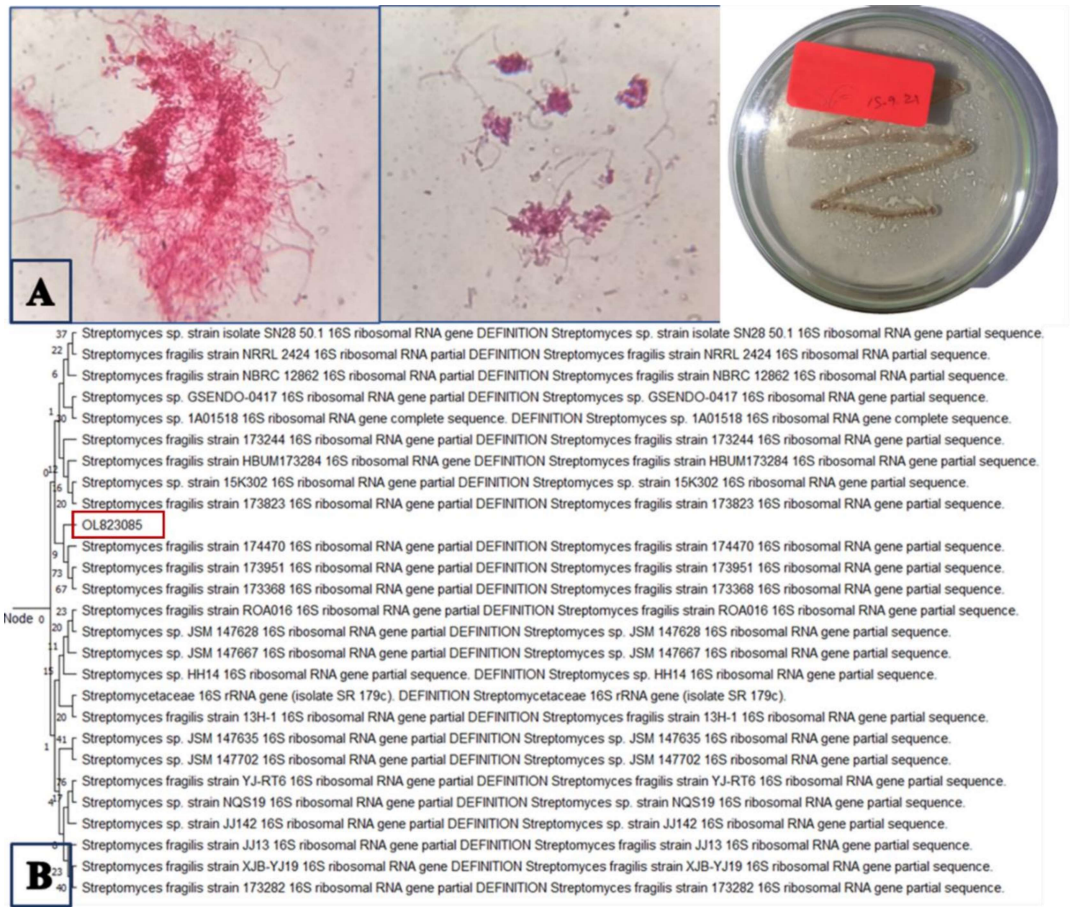

Figure 5.1: The strain characterization. (A) Cultured plate of isolated actinomycetes and its microscopic 100x zoom image, and (B) Phylogenetic relationship tree of the actinomycetes. The isolated strain is highlighted with a red boundary.

The strain was identified as gram-positive based on the Gram stain test. The molecular characterization of the strain was performed by obtaining a 16S rDNA sequence of 1258

bp. Phylogenetic analysis of this sequence, using a dataset of *Streptomyces* genomes, indicated that the strain belongs to the genus *Streptomyces*.

An Inter-genus large dataset of *Streptomyces* is used to build the phylogenetic tree using the Mega11 tool. The resulting phylogeny showed the genomes of different species of *Streptomyces* grouped into their respective clades. This phylogenetic tree shows the common ancestor lineages among the different species of *Streptomyces*. The desired strain number 173823 emerges from the common ancestor (NODE-0) and diverges into sub-different branches. OL823085 lineage clearly diverged among their clades and showed significant similarity within the taxon of the same different branches, like NRRL2424. This result is considered highly conserved and has low evolutionary levels for *Streptomyces fragilis*.

5.3.2 Protein Kinase Inhibitory Assay

This study examined the presence of protein kinase inhibitors (PKI) in the crude extracts of *Streptomyces fragilis* of various media using *Streptomyces 85E* as a model organism. The growth pattern of *Streptomyces 85E* was used as an indicator of the presence or absence of PKI.

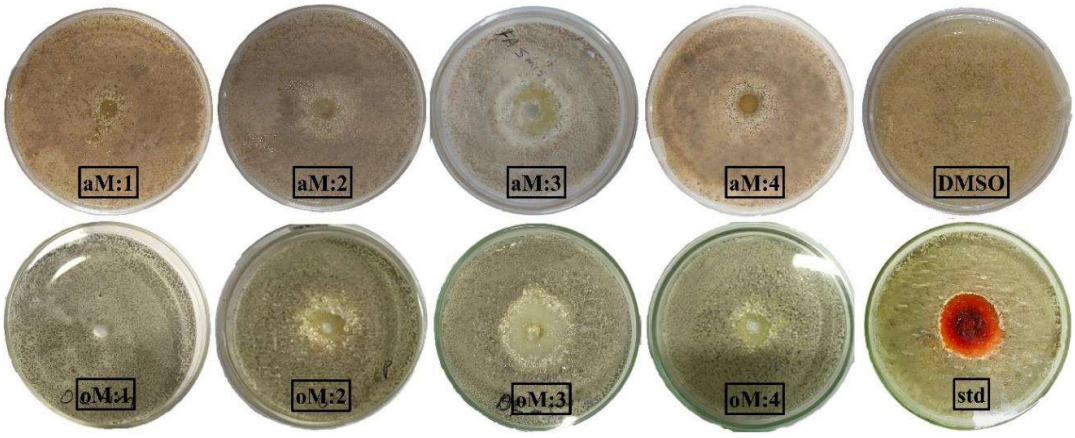

Figure 5.2: Plates labelled as aM:1. aM:2, aM:3, and aM:4 are *Streptomyces*'s aqueous extracts, whereas oM:1. oM:2, oM:3, and oM:4 are organic extracts in respective media. Dimethyl sulfoxide (DMSO) is used as a negative control, and std as doxorubicin, a positive control. Whitish hazy zones indicate the presence of Protein Kinase Inhibitors in the extract, and clear zones indicate complete inhibition of bacteria.

As illustrated in Figure 5.2, test plates without any zone indicate the lack of PKI, a whitish bald zone in plates suggests the presence of PKI in the sample, and a clear zone shows complete inhibition of the growth of strain *Streptomyces 85E*, which may be due to the presence of antimicrobial compounds. Aqueous extract obtained from all media M:2, M:4, and M:3 show the presence of bald zone in the plate with approximately 18 mm, 16 mm, and 24 mm, respectively, and in organic extract, the zone is as M:2: 16 mm, M:4: 11 mm, and M:2: 24 mm whereas M:1 did not show any effect in both extracts. Dimethyl sulfoxide (DMSO) is used as a negative control for the kinase inhibitor activity, and doxorubicin shows complete inhibition of bacteria with a thin, hazy line on the zone edge.

5.3.3 Antioxidant Potential

The DPPH free radical scavenging abilities of *Streptomyces fragilis* extract are depicted in Figure 5.3. Notably, standard antioxidant drug, ascorbic acid, exhibited the most robust scavenging activity, displaying an IC_{50} value of 14.38 ± 0.14 µg/mL.

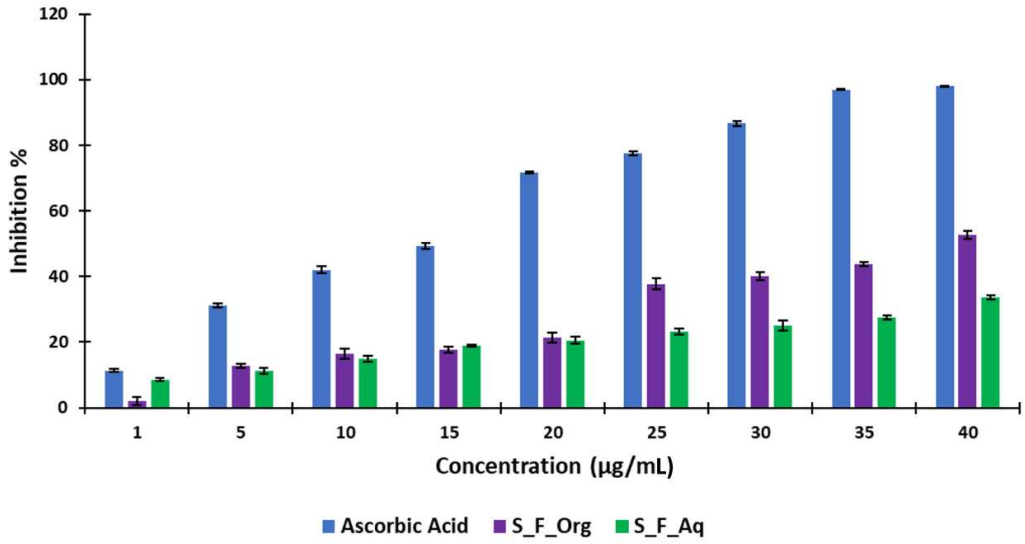

Figure 5.3: free radical scavenging activity of epirubicin and organic (S_F_Org) and aqueous (S_F_Aq) extract of *Streptomyces fragilis*

The organic extract of *Streptomyces fragilis* demonstrated a more potent free radical scavenging capacity (IC_{50} of 38.76 ± 0.39 µg/mL) compared to the aqueous extract (IC_{50}

of 70.68 ± 0.37 µg/mL). However, neither of the extracts exhibited comparable inhibitory effects to those of ascorbic acid.

5.3.4 MTT Assay

Protein kinase and antioxidant assays indicated that the organic extract had superior effects compared to the aqueous extract. Consequently, further experiments were conducted using the organic extract. The efficacy of organic crude extracts of *Streptomyces fragilis* in inhibiting the proliferation of diverse cancer cell lines was assessed through the MTT assay. It was conducted to determine the half-maximal inhibitory concentration (IC_{50}) values for MCF-7, Hop-62, SiHa, and PC-3 cell lines. The findings showed that the organic extract had the most substantial inhibitory effects against the SiHa (58.46 ± 2.0 µg/mL) and MCF-7 (61.14 ± 2.5 µg/mL) cell lines. The IC_{50} values for Hop-62 and PC-3 were 88.26 ± 3.2 µg/mL and 98.92 ± 2.1 µg/mL. The percentage growth of each cell line with varying concentrations of the organic is presented in Figure 5.4.

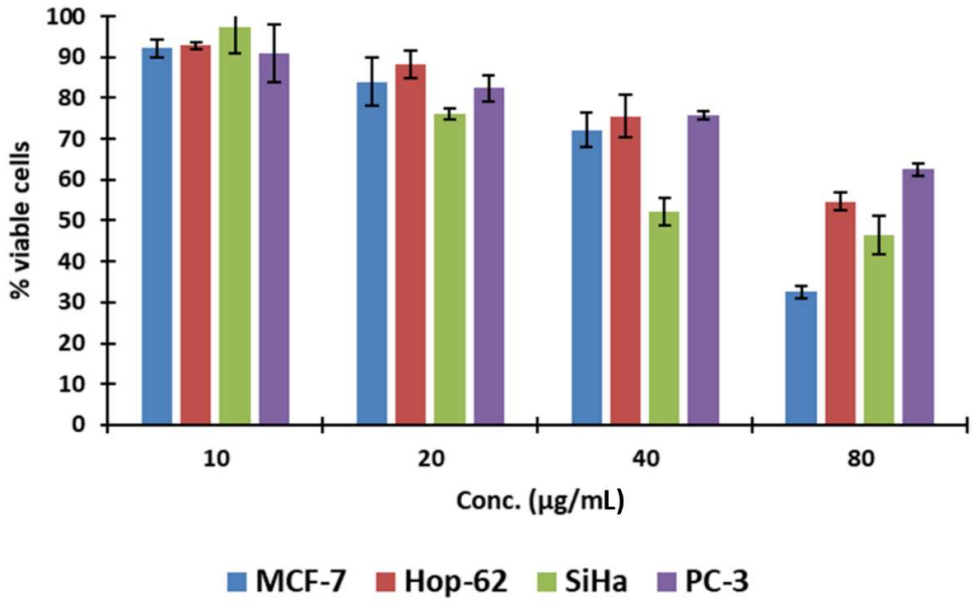

Figure 5.4: Percentage growth of MCF-7, Hop-62, SiHa, and PC-3 cancerous cell lines (cultured at 37 °C temperature, 5:95 of CO2: air composition, and 100% RH for 24 hours) with varying concentrations of the organic *Streptomyces fragilis* extracts.

These findings suggest that further exploration of the organic extract is needed to identify and isolate its active compounds and understand their mechanisms of action. Ultimately, this could lead to the development of novel cancer treatments.

5.3.5 Identification of Secondary Metabolites

The *Streptomyces 85E* assays show good preliminary results of kinase inhibition in batch fermented extract in M:3 media. Further, the chemical composition was checked by HR-LCMS, where the chromatography technique determines the metabolite's composition according to their retention time, m/z, database difference, and proposed compound.

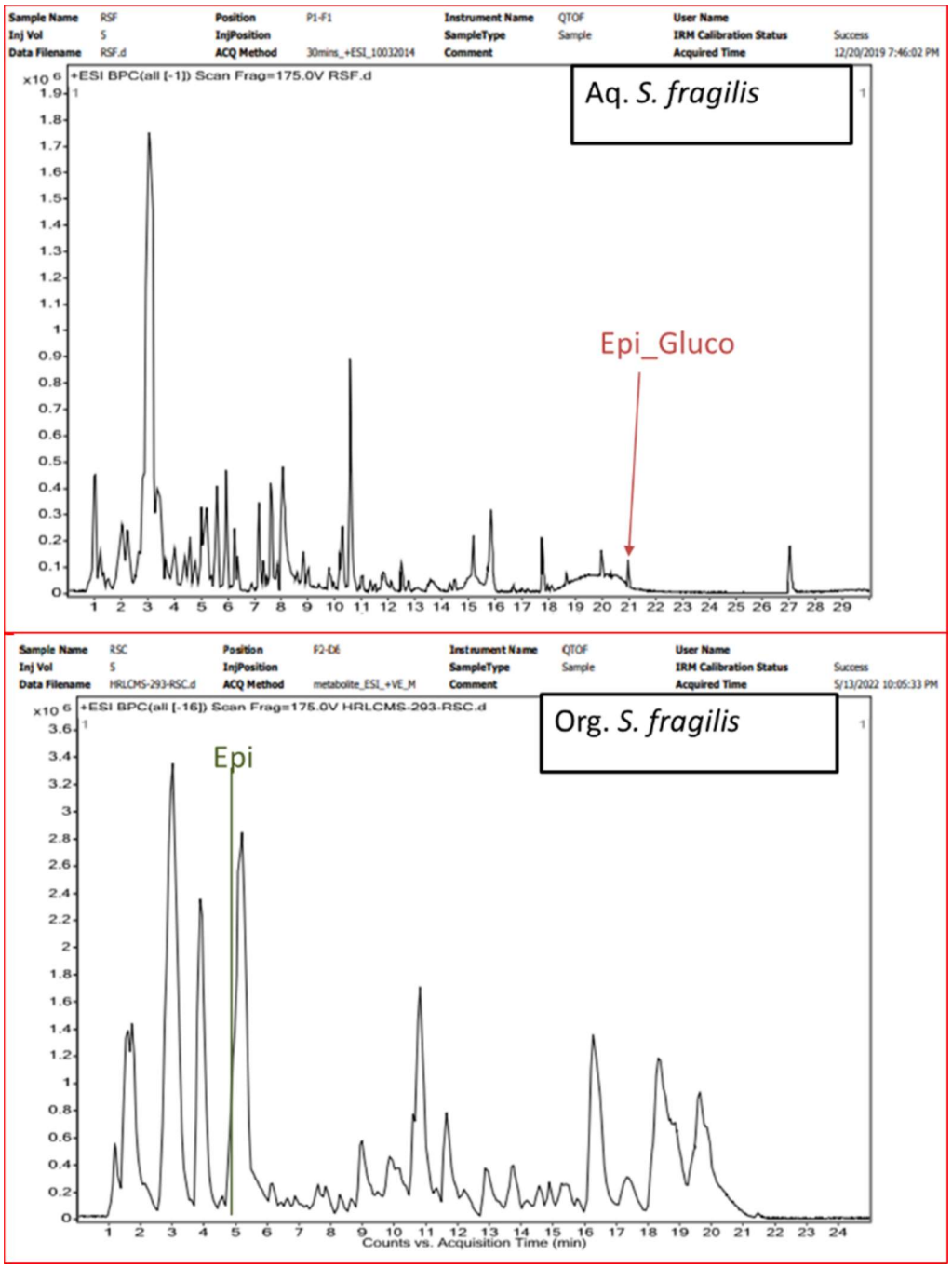

Figure 5.5: HRLCMS chromatogram of aqueous and organic extract of *Streptomyces fragilis* showing a great resolution peak.

The m/z values of secondary metabolites ranged between 158 and 702. HRLCMS chromatogram of aqueous and organic extract of *Streptomyces fragilis* is represented in Figure 5.5. Details of identified secondary metabolites from aqueous and organic extracts are listed in Tables 5.1 and 5.2

Table 5.1: Secondary metabolites identified by the HR-LCMS from the aqueous extract of *Streptomyces fragilis* (extracted from the stationary phase of fermentation, after 72 hrs of incubation period)

Aqueous Extract				
Name	**RT**	**Mass**	**Formula**	**[m/z]**
11Z-heptadecen-1-ol	0.914	254.2586	$C_{17}H_{34}O$	277.2481
3-Prenyl-4-Hydroxyacetophenone	0.934	204.1147	$C_{13}H_{16}O_2$	187.1114
Punctaporin B	0.963	252.168	$C_{15}H_{24}O_3$	275.1584
Ibuprofen	1.049	206.132	$C_{13}H_{18}O_2$	189.1287
Semustine	1.109	247.1106	$C_{10}H_{18}ClN_3O_2$	270.0997
N, N-dimethylhistidine	1.93	183.0995	$C_8H_{13}N_3O_2$	166.0963
Diethyl Oxalpropionate	1.948	202.0829	$C_9H_{14}O_5$	225.0721
Ethenodeoxyadenosine	2.135	275.1021	$C_{12}H_{13}N_5O_3$	276.1094
Nabumetone alcohol	2.792	230.1294	$C_{15}H_{18}O_2$	213.1261
Meperidinic acid	3.085	219.122	$C_{13}H_{17}NO_2$	224.1006
Tranexamic acid	3.176	157.1103	$C_8H_{15}NO_2$	158.1176
11alpha-Acetoxykhivorin	3.279	644.2762	$C_{34}H_{44}O_{12}$	314.1401
deschlorobenzoyl Indomethacin	3.486	205.0768	$C_{11}H_{11}NO_3$	188.0735
Dodecaprenyl phosphate-galacturonic acid	3.751	614.3337	$C_{31}H_{51}O_{10}P$	321.1508
4,8,11,14-Eicosatetraynoic acid	3.861	296.1767	$C_{20}H_{24}O_2$	301.1553
Pentazocine	3.867	285.2063	$C_{19}H_{27}NO$	268.203
Ergonovine	4.179	325.1795	$C_{19}H_{23}N_3O_2$	326.1868
Bilirubin	4.409	584.261	$C_{33}H_{36}N_4O_6$	284.1334
Perindopril glucuronide	4.415	544.2606	$C_{25}H_{40}N_2O_{11}$	567.2507
Netilmicin	4.974	475.3016	$C_{21}H_{41}N_5O_7$	476.3073
Pheniramine	5.383	240.1647	$C_{16}H_{20}N_2$	241.172
Enzacamene	5.521	254.1675	$C_{18}H_{22}O$	259.1461
Panaxydol chlorohydrine	5.551	296.1541	$C_{17}H_{25}ClO_2$	279.1508
Ergoline-1,8-dimethanol, 10-methoxy-, (8b)-	5.902	302.1645	$C_{17}H_{22}N_2O_3$	285.1612
6E,8E,14E-Hexadecatriene-10,12-diynoic acid	6.333	242.1304	$C_{16}H_{18}O_2$	247.1091
8-18 bonded retinal	7.105	282.1978	$C_{20}H_{26}O$	287.1765
3-[(4-Carboxy-4-methylpentyl)oxy]-4-methylbenzoic acid (Gemfibrozil M3)	7.29	280.1311	$C_{15}H_{20}O_5$	285.1097
Buprenorphine	7.335	467.3059	$C_{29}H_{41}NO_4$	450.3047
d-Camphorsulfonate	7.684	232.0784	$C_{10}H_{16}O_4S$	255.0676
Hesperetin	7.697	302.0798	$C_{16}H_{14}O_6$	285.0765
WIN 55212-2	7.803	426.1923	$C_{27}H_{26}N_2O_3$	427.2111
Gentamicin C1a	8.476	449.2852	$C_{19}H_{39}N_5O_7$	432.2819
C16 Sphinganine	9.775	273.268	$C_{16}H_{35}NO_2$	274.2753
Cinnarizine	9.827	368.2229	$C_{26}H_{28}N_2$	369.2302
Oxybutynin	10.01	357.228	$C_{22}H_{31}NO_3$	358.2355

Edoxudine	10.176	256.1051	$C_{11}H_{16}N_2O_5$	279.0944
N,N-Diacetylchitobiosyldiphosphodolichol	10.627	790.2997	$C_{31}H_{56}N_2O_{17}P_2$	387.1551
(-)-Usnic acid	13.75	344.0884	$C_{18}H_{16}O_7$	327.0848
benzonatate(2,5,8,11,14,17,20,23,26-Nonaoxaoctacosan-28-yl p-(butylamino)-benzoate	15.776	603.3748	$C_{30}H_{53}NO_{11}$	604.3824
Tetrahydrogambogic Acid	17.827	632.3355	$C_{38}H_{48}O_8$	637.314
Zopiclone	18.644	388.1108	$C_{17}H_{17}ClN_6O_3$	371.1087
DL-PDMP	20.37	390.2845	$C_{23}H_{38}N_2O_3$	391.2919
Epirubicin glucuronide	20.941	719.2127	$C_{33}H_{37}NO_{17}$	702.2124
14-hydroxy-5Z-tetradecenoic acid	26.986	242.1885	$C_{14}H_{26}O_3$	247.1672
Prometon	27.11	225.1557	$C_{10}H_{19}N_5O$	230.1343

Table 5.2: Secondary metabolites identified by the HR-LCMS from the organic extract of *Streptomyces fragilis* (extracted from the stationary phase of fermentation, after 72 hrs of incubation period)

Organic Extract				
Name	RT	Mass	Formula	[m/z]
Retronecine	1.134	155.0946	$C_8H_{13}NO_2$	156.1019
2-C-Methyl-D-erythritol 4- phosphate	1.138	216.0406	$C_5H_{13}O_7P$	215.0352
Sulochrin	1.175	332.0895	$C_{17}H_{16}O_7$	377.0897
p-Mentha-1,3,5,8-tetraene	1.607	132.0921	$C_{10}H_{12}$	155.0814
Aprobarbital	1.608	210.0999	$C_{10}H_{14}N_2O_3$	211.1071
5-Hydroxykynurenamine	1.853	180.0894	$C_9H_{12}N_2O_2$	181.0966
Anisessine	1.931	349.1426	$C_{20}H_{19}N_3O_3$	372.1341
6-Hydroxypseudooxynicotine	2.692	194.1051	$C_{10}H_{14}N_2O_2$	195.1123
Fasoracetam	3.792	196.1206	$C_{10}H_{16}N_2O_2$	197.1278
Fluoroacetaldehyde	4.633	62.0167	C_2H_3FO	121.0305
L,L-Cyclo(leucylprolyl)	4.791	210.1363	$C_{11}H_{18}N_2O_2$	211.1436
8-Methoxykynurenate	4.856	219.0557	$C_{11}H_9NO_4$	218.0484
Epirubicin	4.972	543.1562	$C_{27}H_{29}NO_{11}$	566.1613
Bisphenol A dimethacrylate	5.218	364.1682	$C_{23}H_{24}O_4$	183.0914
Azobenzene	5.522	182.0842	$C_{12}H_{10}N_2$	183.0915
(3R,7R)-1,3,7-Octanetriol	6.113	162.1256	$C_8H_{18}O_3$	185.1143
4-Hydroxy-3-methyl benzoic acid	6.641	152.0492	$C_8H_8O_3$	151.042
4-Ethyl-2-heptylthiazole	6.795	211.136	$C_{12}H_{21}NS$	212.1428
2,3,5-Trimethyl-6-[4-(methylthio)butyl]pyrazine	7.015	224.1308	$C_{12}H_{20}N_2S$	225.138
gamma-Chaconine	7.554	559.3843	$C_{33}H_{53}NO_6$	560.3914
Diethyltoluamide	8.316	191.1306	$C_{12}H_{17}NO$	192.1378

Vulgarone A	8.634	218.1665	$C_{15}H_{22}O$	219.1737
Dihydrocapsaicin	8.871	307.2133	$C_{18}H_{29}NO_3$	308.2206
(+)-Ligballinol	8.882	298.1237	$C_{18}H_{18}O_4$	297.1164
N-(2,14-Eicosadienoyl) piperidine	8.939	375.3511	$C_{25}H_{45}NO$	398.3399
9,10-Dihydroxy-12,13- epoxyoctadecanoate	9.119	330.2447	$C_{18}H_{34}O_5$	329.2374
3-Epidemissidine	9.192	399.3476	$C_{27}H_{45}NO$	400.3549
Trimethobenzamide	9.245	388.2013	$C_{21}H_{28}N_2O_5$	387.1961
Drospirenone	9.279	366.2196	$C_{24}H_{30}O_3$	365.2137
9,10,13-trihydroxy-11- octadecenoic acid	9.372	330.2392	$C_{18}H_{34}O_5$	353.2282
U 0521	9.474	180.0803	$C_{10}H_{12}O_3$	179.0731
Eudesobovatol A	9.5	504.3245	$C_{33}H_{44}O_4$	505.332
Avenestergenin B2	9.597	592.3767	$C_{37}H_{52}O_6$	593.3841
4-(3,5-Diphenylcyclohexyl)phenol	10.42	328.1832	$C_{24}H_{24}O$	387.1961
Nilvadipine	10.458	385.1304	$C_{19}H_{19}N_3O_6$	408.1197
17-Hydroxylinolenic acid	10.894	294.2186	$C_{18}H_{30}O_3$	295.2256
Tetradecyl sulfate	10.904	294.1871	$C_{14}H_{30}O_4S$	293.1798
Mercaptoacetyl-Phe-Leu	10.991	352.1453	$C_{17}H_{24}N_2O_4S$	351.1384
Procarbazine	11.139	221.1577	$C_{12}H_{19}N_3O$	220.1495
Sphinganine	11.581	301.2969	$C_{18}H_{39}NO_2$	302.3042
Myristic acid	11.649	228.2102	$C_{14}H_{28}O_2$	251.1995
Nigakilactone B	11.816	392.2205	$C_{22}H_{32}O_6$	415.2096
Asterosterol	12.897	370.3177	$C_{26}H_{42}O$	371.325
Guazatine	13.159	355.3435	$C_{18}H_{41}N_7$	356.3506
Lauric acid	13.805	200.1795	$C_{12}H_{24}O_2$	223.1688
Rishitin	13.855	222.1644	$C_{14}H_{22}O_2$	221.1571
8S-Hode	13.898	296.2389	$C_{18}H_{32}O_3$	295.2317
9-Hote	14.139	294.223	$C_{18}H_{30}O_3$	293.2158
3-keto stearic acid	14.381	298.2543	$C_{18}H_{34}O_3$	297.247
Jamaicamide C	15.261	490.2545	$C_{27}H_{39}ClN_2O_4$	535.2526
Hexazinone	15.684	252.1583	$C_{12}H_{20}N_4O_2$	297.1566
Lauryl hydrogen sulfate	16.546	266.1586	$C_{12}H_{26}O_4S$	265.1514
all-trans-hexaprenyl diphosphate	18.271	586.3198	$C_{30}H_{52}O_7P_2$	645.3342
Hydroquinidine	18.442	326.1959	$C_{20}H_{26}N_2O_2$	325.1889
Proparacaine	19.441	294.191	$C_{16}H_{26}N_2O_3$	353.2053
(3beta,22E,24R)-3-Hydroxyergosta-5,8,22-trien-7- one	19.897	410.3236	$C_{28}H_{42}O_2$	409.3163
4-Dodecylbenzenesulfonic acid	20.61	326.1958	$C_{18}H_{30}O_3S$	325.1885

5.3.6 Molecular Docking

Molecular docking and molecular dynamics simulation were performed to elucidate the inhibitory potential of secondary metabolites identified from *Streptomyces fragilis* against various protein kinase targets. A mutation in protein kinase genes is one of the reasons for cancer development and progression. So, different types of protein kinase BCL-2, BCR-ABL, CDK4, EGFR, JAK2, PDGFR, and PI3K having a mutation at a specific place were selected to find their inhibitors and develop a drug against cancer. Only PI3K was exhibited without any mutation among the targeted proteins. The secondary metabolites of *S. fragilis* identified from HR-LCMS analysis were subjected to a molecular docking study with these kinase proteins. Among all the secondary metabolites of *S. fragilis*, the frequency of epirubicin displays better binding energy with protein BCL-2, CDK4, EGFR, and PDGFR. Therefore, epirubicin was chosen as a drug of interest to study its binding and inhibitory potential over all these proteins, and doxorubicin was taken as the standard drug.

Docking results revealed that when the drug of interest, epirubicin, docked with CDK4 protein kinase, it demonstrated a robust binding interaction with the CDK4 kinase protein by forming five hydrogen bonds with the residues Val96, Arg101, Ile12, Gly15, and Asp158 with the binding score – 10.40 Kcal/ mol. Meanwhile, the standard drug doxorubicin formed only three H-bonds with Arg101, Glu94, and Asp158 amino acids of CDK4 protein with a significantly less binding affinity (-5.953 Kcal/ mol) as given in Table **5.3.**

Table 5.3: Binding energy and Hydrogen interaction analysis of epirubicin and standard drug Doxorubicin with various types of kinase protein

Target	Epirubicin		Standard (Doxorubicin)	
	Binding Energy (Kcal/mol)	H-Bond interaction	Binding Energy (Kcal/mol)	H-Bond interaction
BCL2	-7.183	Arg105, Asp99, Glu95, Phe71	-5.595	Asp99, Asp 70

BCR-ABL	-6.318	Asp381, Ile360, Arg362	-6.301	Glu282, Ile360
CDK4	-10.401	Val96, Arg101, Ile12, Gly15, Asp158	-5.953	Arg101, Glu94 and Asp158
EGFR	-8.677	Glu762	-8.881	Glu762
JAK2	-7.527	Pro839, Leu840	-5.020	Asn923, Arg1051
PDGFR	-11.501	Leu599, Cys677, Tyr679	-9.301	Phe678, Cys677, Arg597
PI3K	-6.738	Ala805, Ala885	-8.272	Ala885, Ala805, Asp950.

The stable interaction created by epirubicin can be explained by the shift in the orientation of one oxygen atom in the daunosamine ring (ring D), which brings the oxygen atom closer to Ile12 and Val96 for forming a hydrogen bond as presented in **Figure 5.6**.

As shown in Table 5.3, epirubicin also showed better binding energy with Bcl2, JAK2, and PDGFR kinase protein. It interacted with Bcl2 kinase by three hydrogen bonds with Arg105, Asp99, Glu95, and pi–pi interaction with Phe71, while doxorubicin interacted with Bcl2 kinase via two hydrogen bonds with Asp99, Asp70. Epirubicin displayed an H-bond with the active site amino acid residues Pro839 and Leu840 of JAK2 protein via its OH group of daunosamine groove and the OH group of anthraquinone moiety acting as hydrogen bond donors. In contrast, doxorubicin interacted with JAK2 at Asn923 and Arg1051. The daunosamine ring (ring D) of doxorubicin and epirubicin in the JAK2 case was structured differently, which caused the OH-group and NH2 group to be oriented differently, as illustrated in **Figure 5.7**. Epirubicin made a hydrogen bond with the Pro839 residue, but due to that orientation, the NH2 group of epirubicin did not make a hydrogen bond with Arg1051 of the JAK2 receptor.

Epirubicin formed a hydrogen bond with Leu599, Cys677, and Phe678 residues of the receptor PDGFR, where Leu599 and Phe678 functioned as hydrogen acceptors, while Cys677 performed as a hydrogen donor. In contrast, doxorubicin interacted with PDGFR at Phe678, Cys677, and Arg597 residues.

Epirubicin interacted with PI3K at hydrogen bond acceptor residues Ala885 and Ala805 through its NH2 moiety of daunosamine groove and OH group of anchor region with a

binding score of -6.738. The better binding interaction was expressed by doxorubicin with PI3K through a hydrogen bond at Ala885, Ala805, and Asp950, with a binding energy of -8.272.

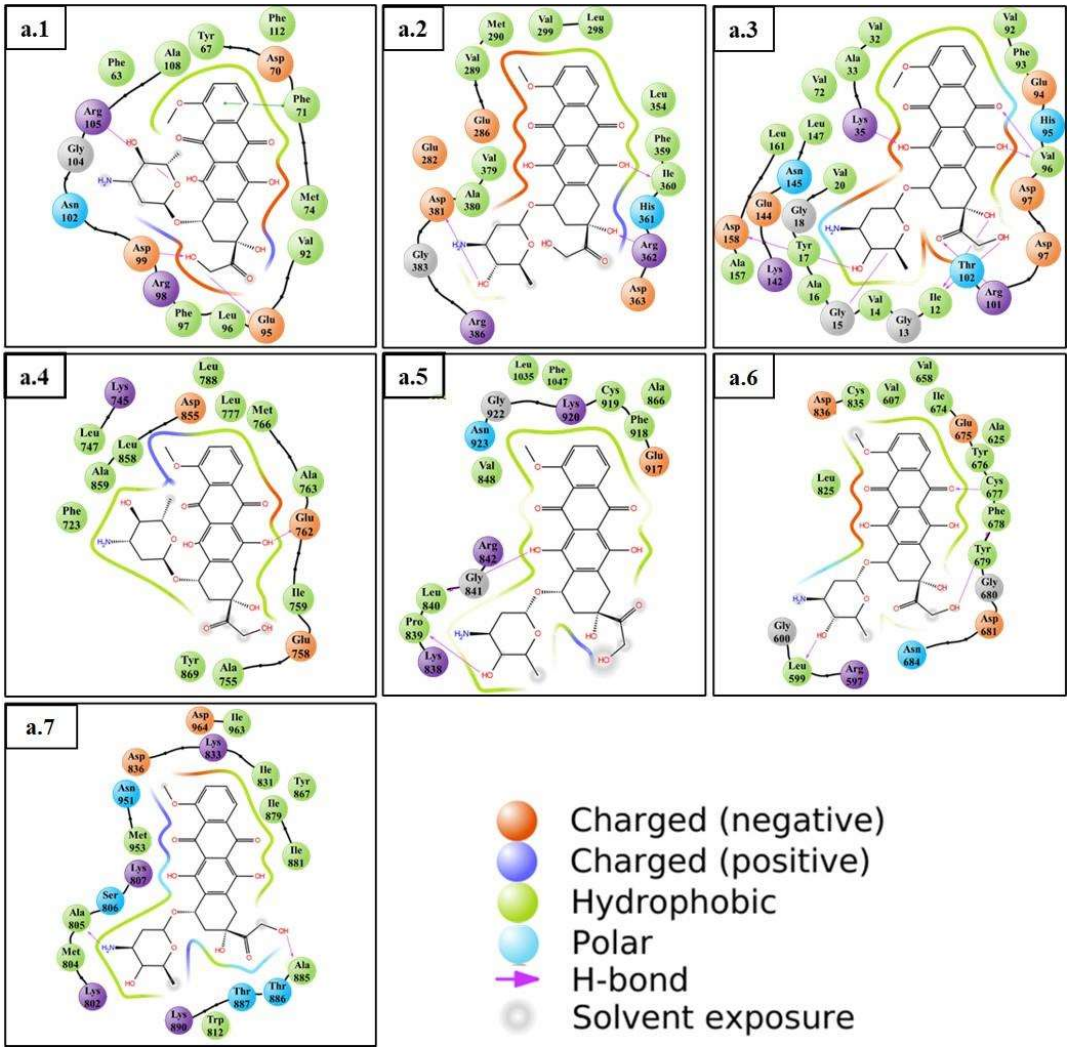

Figure 5.6: 2D Molecular docking interactions of epirubicin with various target proteins, represented as a.1: BCL2, a.2: BCR-ABL, a.3: CDK4, a.4: EGFR, a.5: JAK2, a.6: PDGFR, a.7: PI3K.

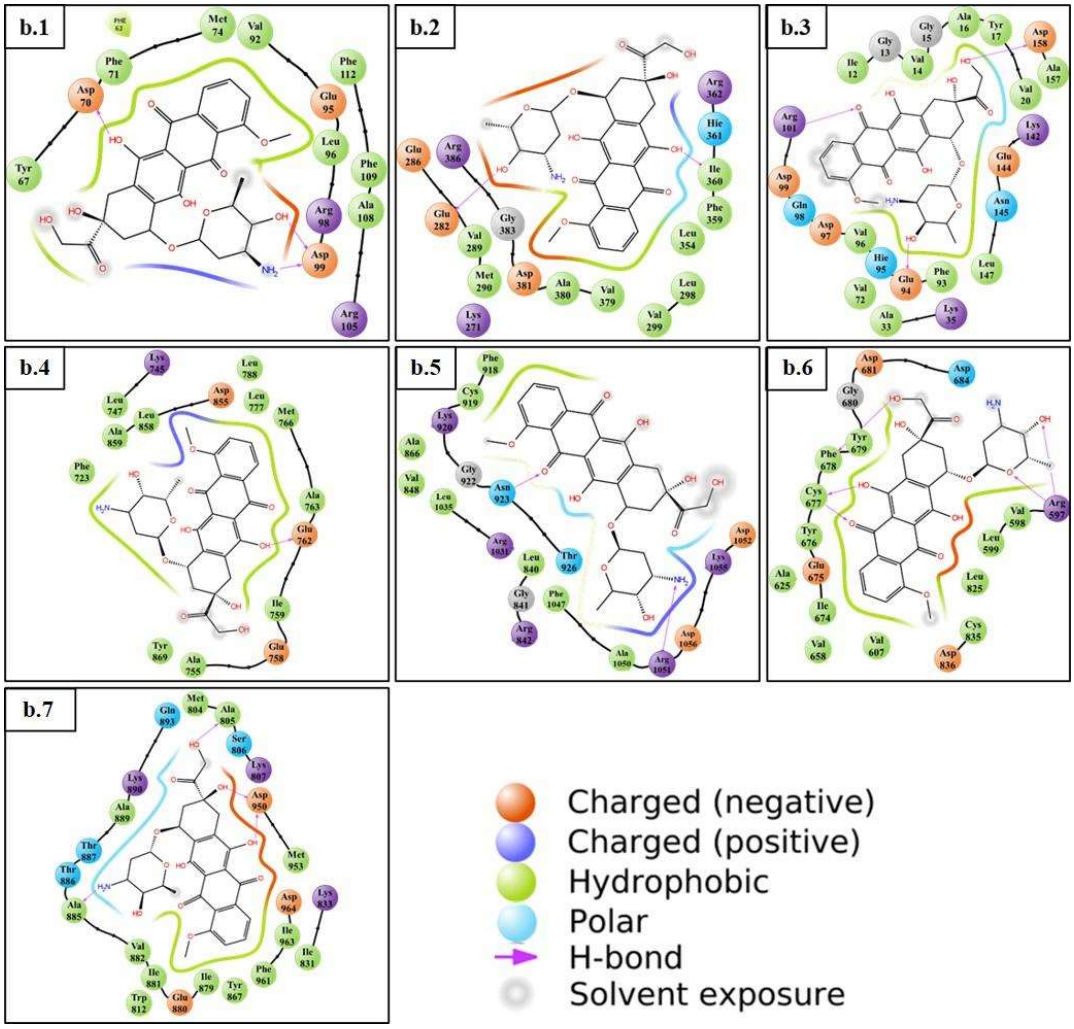

Figure 5.7: Molecular docking interactions of doxorubicin with various target proteins, represented as b.1: BCL2, b.2: BCR-ABL, b.3: CDK4, b.4: EGFR, b.5: JAK2, b.6: PDGFR, b.7: PI3K.

The more stable binding interaction exhibited by doxorubicin with PI3K was caused by the fact that the majority of the portion of doxorubicin was located in the binding pocket of both proteins, as depicted in **Figure 5.7.**

Doxorubicin showed H-bond interaction with BCR-ABL at Glu282 and Ile360 residues with a binding score of -6.301. At the same time, epirubicin interacted with hydrogen bond acceptor Asp381, Ile360, and hydrogen donor Arg362 residue, with similar binding energies of -6.318. In addition, doxorubicin and epirubicin drugs interacted with EGFR at Glu762 through the anthraquinone ring, which acted as hydrogen donors and showed

similar binding scores of -8.677 and -8.881, respectively. **Table 5.3** displays the binding score and hydrogen bond-forming amino-acid residues of the kinase protein with the hit drug epirubicin and the standard drug doxorubicin.

Therefore, based on the binding energy and molecular interaction acquired from molecular docking, except PI3K, the ligand epirubicin revealed better binding potential than standard doxorubicin; however, with four kinase proteins BCL2, CDK4, JAK2, and PDGFR it expressed better inhibitory ability than Doxorubicin drug and with BCL-ABR, and EGFR kinase its inhibitory potential was very comparable with the standard.

5.3.7 Molecular Dynamics Simulation

Molecular docking only provides a preliminary understanding of how proteins and ligands interact. Therefore, in order to verify the docking results and to discover the stability and dynamics of the ligand-protein complex, a molecular dynamics simulation was conducted for 200 ns. **Figure 5.8** illustrates the RMSD, SASA, rGyr, and number of H-bonds of all kinase proteins in the Apo state, in complex with epirubicin and standard drug doxorubicin.

It showed that the average RMSD value of all apo protein ranges from 2.08 to 4.04, and for epirubicin in complex with all proteins, the value ranges from 1.95 to 4.44, which is relatively lower with respect to doxorubicin (1.94 to 5.28). As shown in **Figure 5.8,** EGFR protein initially displayed stability up to 120 ns, then fluctuated from 130 to 170 ns and regained equilibrium. The epirubicin combination with BCR-ABL, JAK2, PDGFR, PI3K, and BCL2 showed stability throughout the simulation and was substantially similar to doxorubicin. CDK4 protein displayed fluctuation up to 30 ns, after which it became highly stable throughout the MD simulation when complexed with epirubicin. In contrast, in complex with doxorubicin, it showed a minor fluctuation throughout the entire simulation process.

The SASA profile of the epirubicin and doxorubicin revealed that the average SASA values of epirubicin were shallow and determined to be equivalent to doxorubicin. The similarity and low SASA value were due to the comparable sizes and structures of both drugs, and a larger portion of the drug remained engulfed in the binding pocket of the protein, where it is inaccessible to solvents. Due to similar chemical structures, the radius of gyration of doxorubicin and epirubicin was also identical, as shown in **Figure 5.8.** Their average rGyr varied between 4.67-4.85 and 4.56-4.84, respectively, and both were displayed in folded and compact forms due to their larger size.

The number of H-bonds formed during the simulation by the residues of the kinase protein with epirubicin and doxorubicin was assessed in **Figure 5.8.** It was revealed that epirubicin formed more hydrogen bonds (1-6) than doxorubicin (1-4) with the BCL2 and BCR-ABL kinase protein residues. Epirubicin generated 1-11 hydrogen bonds, while doxorubicin developed only 1-6 hydrogen bonds with EGFR. During interaction with JAK2, PDGFR, and PI3K proteins, epirubicin initially formed an average of 4 hydrogen bonds and then increased to 12. On the other hand, doxorubicin generated 1-6 hydrogen bonds with JAK2 and PDGFR protein and 1-9 H-bond with PI3K protein throughout the simulation. Epirubicin formed only 1-7 bonds, while doxorubicin formed more H-bonds (2-10) with the CDK4 protein. Therefore, except for the CDK4 kinase protein, epirubicin generated more hydrogen bonds with the BCL2, BCR-ABL, EGFR, JAK2, PDGFR, and PI3K kinase than doxorubicin.

The RMSF of all kinase proteins in the Apo state, in combination with epirubicin and doxorubicin, is shown in **Figure 5.9**. It revealed that, except for the residue Glu42, none of the BCL2 residues that interact with epirubicin fluctuated during the simulation, and this fluctuation is comparable to that of doxorubicin. The presence of epirubicin induced the Met278, Glu282, and Leu284 residues of the BCR-ABL protein to fluctuate less,

indicating that the active site residue of the BCR-ABL kinase was more stable when bound to epirubicin than to doxorubicin, as represented in **Figure 5.9**.

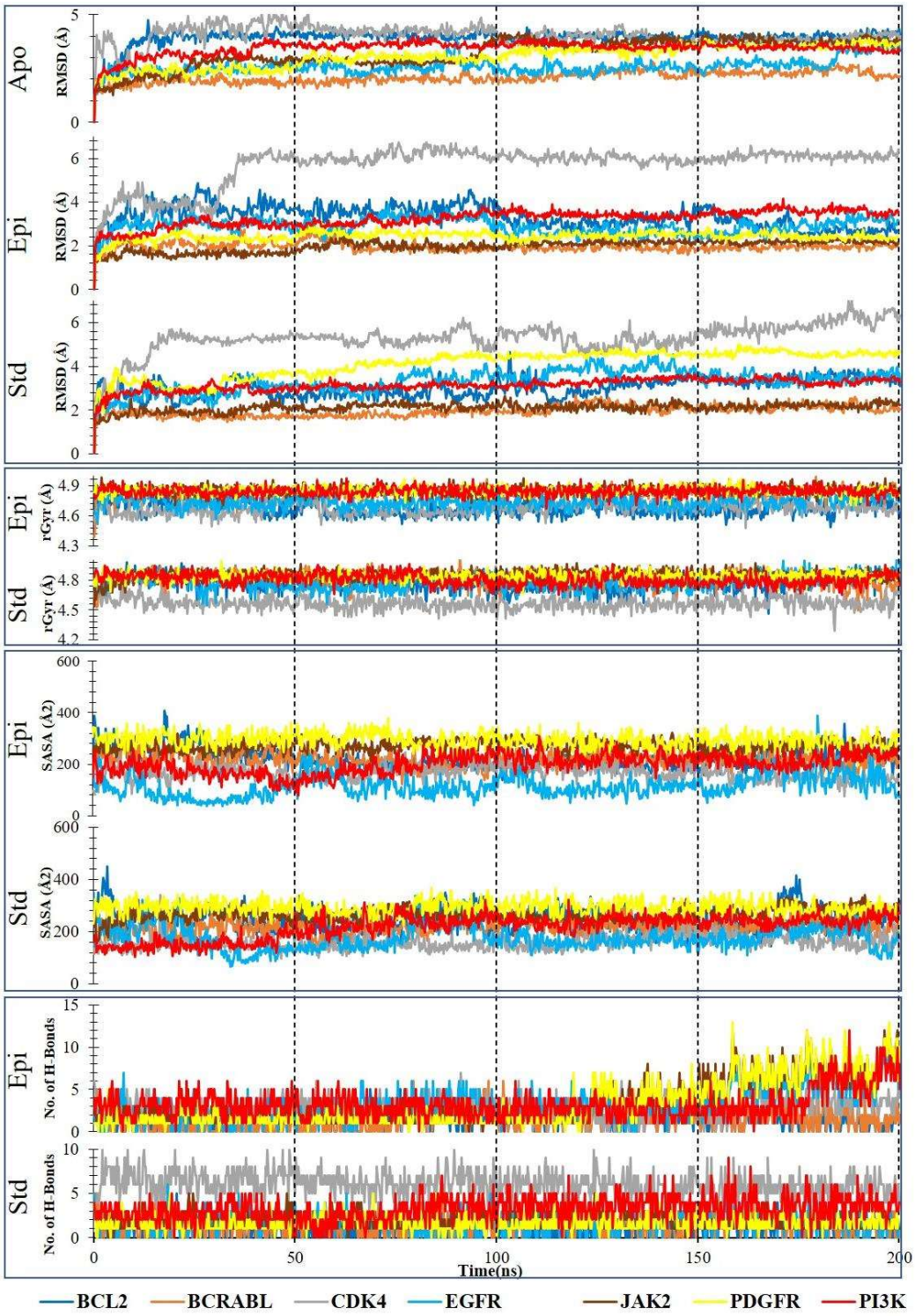

Figure 5.8: RMSD, rGyr, SASA, and Number of Hydrogen Bond formation profiles of respective ten targets in Apo state, in Epi (protein with epirubicin), and Std (protein with doxorubicin) during Molecular Dynamics.

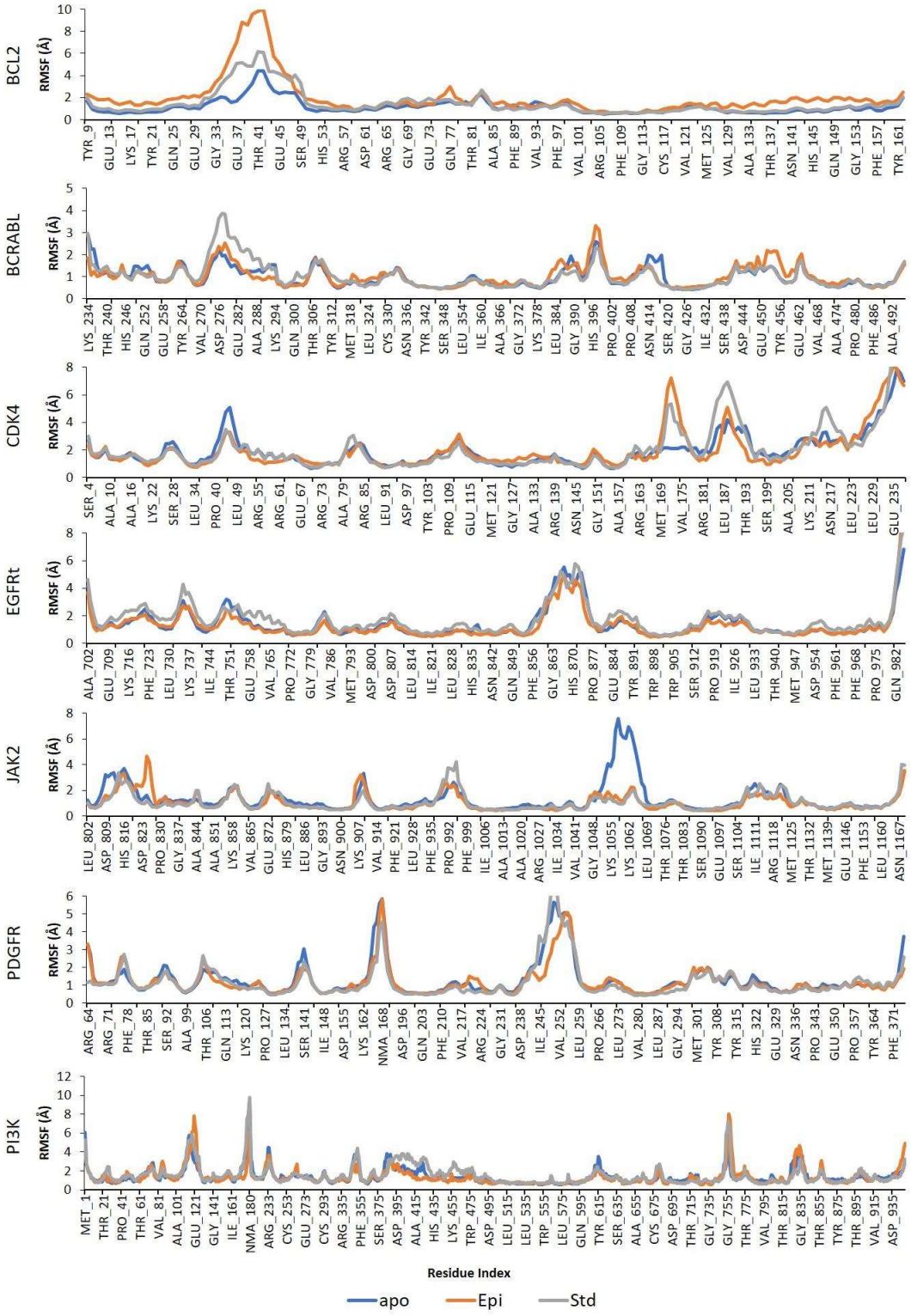

Figure 5.9: Root Mean Square Fluctuation (RMSF) in the amino acid residue of respective target proteins with ligand during Molecular Dynamics simulation of 200 ns.

RMSF values of CDK4 in complex with epirubicin were very comparable to CDK4 + doxorubicin and showed fluctuation at similar residues, although residue Leu187 and

Gly216 of CDK4 indicated higher instability in the case of doxorubicin. All the residues of EGFR fluctuated more when they interacted with doxorubicin and fluctuated less when they interacted with epirubicin. The amino acid residues of JAK2 and PI3K interacting with epirubicin revealed a stable and comparable RMSF to doxorubicin throughout the simulation. For PDGFR kinase protein, the Ser249 amino acid exhibits more fluctuation when associated with doxorubicin than epirubicin.

5.3.8 Protein-Ligand Interaction

Figure 5.10 and Figure 5.11 display the 2D plot illustrating the interaction of epirubicin and doxorubicin with the interacting residues of protein kinase and their interaction% throughout the simulation of 200 ns. MD simulation revealed that epirubicin strongly interacted with BCL2 protein via Arg105, Leu96, and Glu73 with interaction probabilities of 37%, 58%, and 39%, respectively, and water-mediated interaction with Asp99 by 56% probability; however, the standard drug doxorubicin did not form any hydrogen bond with BCL2. Neither doxorubicin nor epirubicin developed any H-bonds with the residues of the BCR-ABL kinase protein. While interacting with the CDK4, epirubicin, and doxorubicin established a common hydrogen bond with Lys35, Asp158, and Glu144 residues, with almost equal interaction probability. Doxorubicin additionally formed a hydrogen bond with Val96, His95, Ala62, and a pi-pi interaction with Arg101 residues of the CDK4 protein.

Doxorubicin had a weak interaction (36%) with EGFR protein through Gly863, but epirubicin showed a strong linkage (51%) through Glu865. For JAK2, both doxorubicin and epirubicin created a strong hydrogen bond with Cys919 with a 98% and 96% hydrogen bond probability, respectively. In addition, doxorubicin also generated an interaction with Pro839 with a 42% interaction probability. With the kinase protein PDGFR, epirubicin exhibited interaction with Cys151 (91%) and Phe152 (31%), whereas

doxorubicin interacted with Cys677 (70%) and Phe678 (30%). Epirubicin interacted with PI3K through two pi-pi interactions with Tyr725 and Trp670 residues and one H-bond interaction with Val740 residues, while doxorubicin interacted only with the Val882 residue of the PI3K protein. Accordingly, the results of the MD simulation demonstrated that the target ligand epirubicin has a better inhibitory potential than doxorubicin for the kinase proteins CDK4, EGFR, PDGFR, and PI3K, and comparable binding potential for BCR-ABL, but for protein BCL2 and JAK2, epirubicin did not reveal better inhibitory activity than doxorubicin.

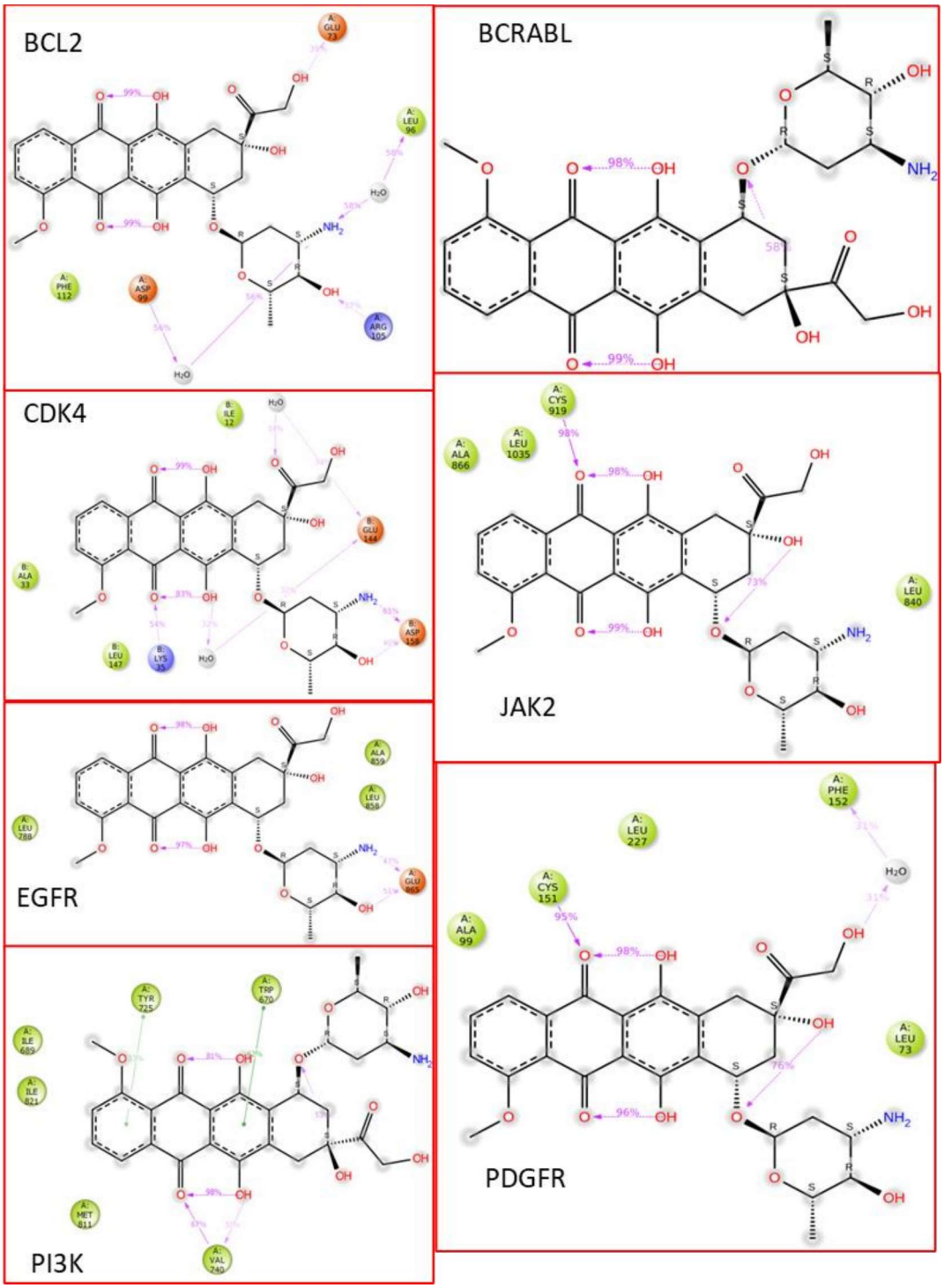

Figure 5.10: The 2D plot showcases the interaction patterns and corresponding percentages of epirubicin with protein kinase residues during a 200 ns molecular dynamics (MD) simulation. The figures label represents specific target proteins as BCL2 (a.1), BCR-ABL (a.2), CDK4 (a.3), EGFR (a.4), JAK2 (a.5), PDGFR (a.6), and PI3K (a.7). These plots provide valuable insights into the binding interactions between epirubicin and the target proteins, offering potential avenues for targeted drug design and optimization.

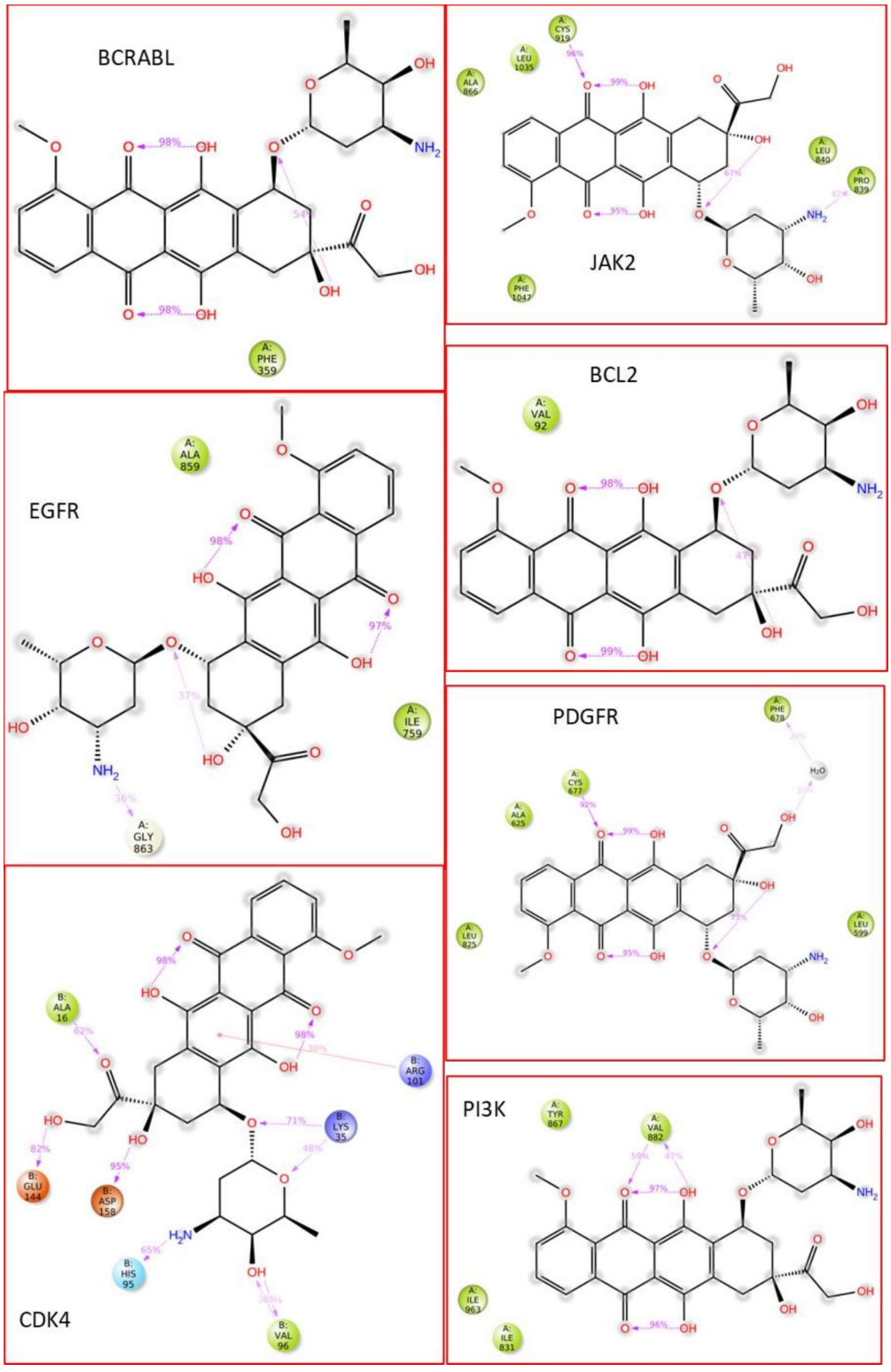

Figure 5.11: The 2D plot represents the interaction of doxorubicin with protein kinase residues and their corresponding interaction percentages during a 200 ns molecular dynamics (MD) simulation. The figures label represents specific target proteins as BCL2 (a.1), BCR-ABL (a.2), CDK4 (a.3), EGFR (a.4), JAK2 (a.5), PDGFR (a.6), and PI3K (a.7). These 2D plots provide insights into the binding dynamics of doxorubicin with protein kinases.

5.3.9 MM/GBSA calculation

To further confirm the inhibitory potential of epirubicin against kinase protein, the binding free energies of epirubicin in complex with kinase protein and standard (doxorubicin)+kinase protein were calculated using the MM/GBSA method. The results of the last 20 ns molecular dynamics simulation trajectories are represented in **Table 5.4.** It was observed that the binding free energy of epirubicin complex with CDK4, EGFR, PDGFR, and PI3K kinase protein was better than that of the standard drug. However, for the proteins BCL2, BCR-ABL, and JAK2, the binding free energies of doxorubicin and epirubicin were equivalent. The van der Waals and lipophilic energy of epirubicin and doxorubicin displayed the same trend as all kinase proteins' total binding free energy, as represented in **Table 5.4.**

Table 5.4: Free energy analysis of epirubicin and doxorubicin complex with target kinase protein on the last 20 ns simulation frames.

	Target	ΔG_{bind}	$\Delta E_{coulomb}$	H-bond	ΔE_{lipo}	ΔE_{ele}	ΔE_{vdw}
Epirubicin	BCL2	-37.32	-10.00	-0.91	-12.52	17.02	-32.04
	BCR-ABL	-45.51	-8.71	-0.41	-16.42	18.71	-39.13
	CDK4	-73.08	-17.22	-3.44	-21.72	28.25	-60.98
	EGFR	-45.78	-9.59	-1.17	-15.80	18.87	-39.38
	JAK2	-49.21	-7.01	-1.00	-15.68	12.28	-39.06
	PDGFR	-65.17	-15.38	-1.78	-21.33	23.07	-52.06
	PI3K	-71.60	-12.99	-1.85	-26.71	21.87	-52.75
Standard	BCL2	-39.62	-11.55	-0.87	-13.44	18.92	-32.88
	BCR-ABL	-46.18	-9.23	-0.64	-16.38	18.83	-39.50
	CDK4	-49.38	-27.17	-3.71	-12.36	34.05	-43.80
	EGFR	-34.90	-5.68	-0.53	-11.30	10.56	-29.21
	JAK2	-52.76	-8.44	-1.05	-16.98	11.75	-39.36
	PDGFR	-51.03	-11.90	-1.37	-16.54	17.90	-40.63
	PI3K	-43.15	-10.80	-1.32	-15.47	15.50	-31.20

5.3.10 Per-residue Decomposition

Furthermore, the energy contribution of each residue in receptor-ligand interaction was evaluated, and the outcomes are depicted in **Figure 5.12**. The residues with binding free energy values below -1 Kcal/mol exhibited a critical and indispensable role in stabilizing the complex. Per residue decomposition analysis also validated the MM/GBSA results and confirmed the superior interaction of epirubicin with receptor CDK4, EGFR, PDGFR, and PI3K compared to the standard drug doxorubicin.

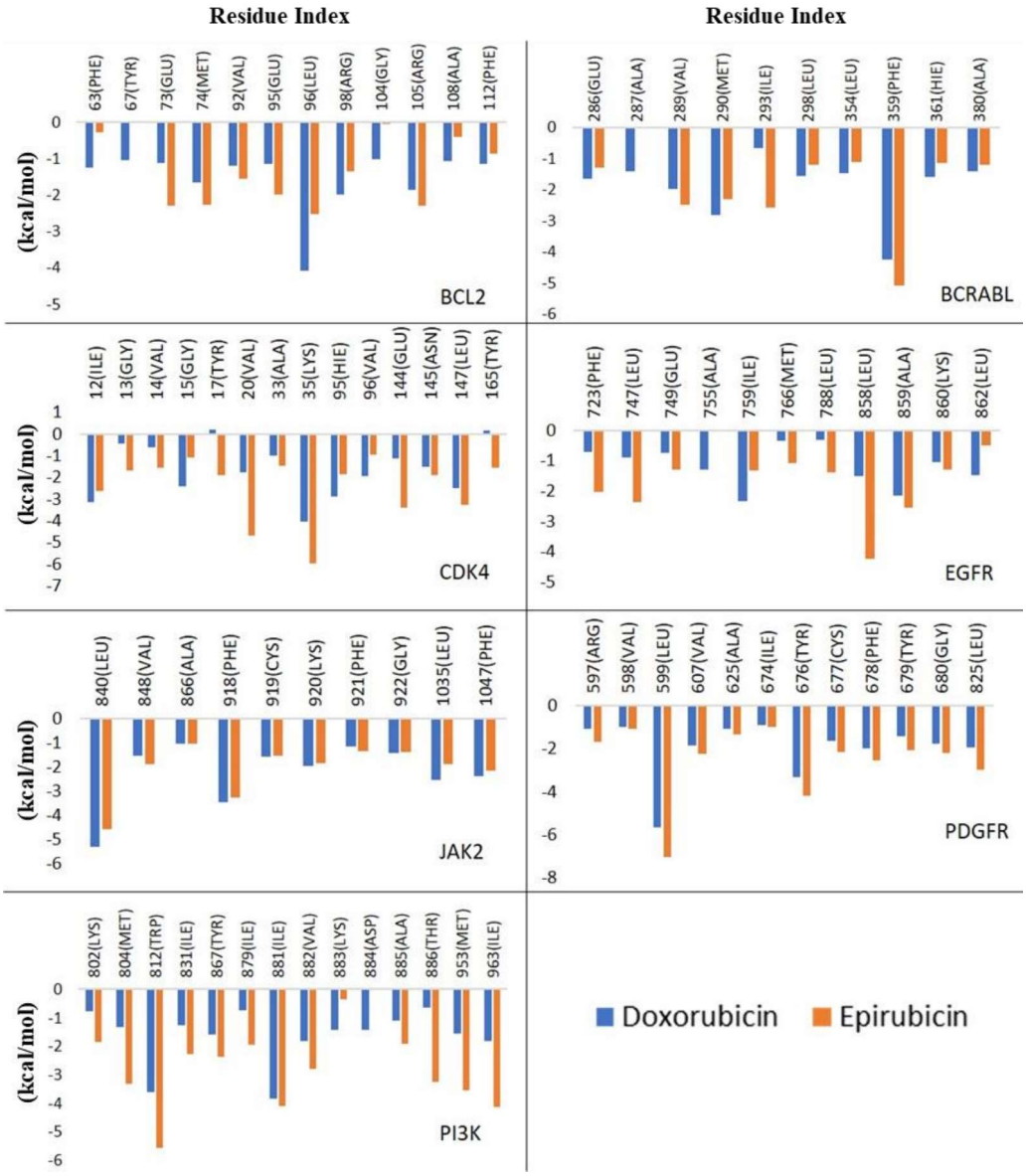

Figure 5.12: Residues and their energy decomposition within a protein-ligand complex structure.

Notably, the residues Val20, Lys35, Glu144, and Leu147 of the CDK4 kinase protein exhibited a significant contribution to the binding of epirubicin, surpassing that of doxorubicin, as illustrated in **Figure 5.12.** In the context of the EGFR receptor, the residues Leu858, Ala859, Leu788, Phe723, and Leu747 displayed crucial roles in ligand binding and demonstrated significantly stronger binding free energy with epirubicin compared to doxorubicin. For PDGFR and PI3K kinase proteins, all residues contributed substantially to the ligand binding process, with a more pronounced energetic contribution observed for epirubicin. Overall, the outcomes derived from the per-residue decomposition analysis provide robust validation for the MM/GBSA findings, confirming the enhanced interaction and more favorable binding energetics of epirubicin compared to doxorubicin with the aforementioned receptors.

5.4 Conclusion

In the current chapter, a strain of *Streptomyces* was isolated, namely strain *Streptomyces fragilis,* which exhibited unique characteristics, including distinctive sporulation and the formation of both vegetative and aerial mycelium, along with abundant growth. It was identified as gram-positive based on gram-staining and further confirmed through molecular characterization using a 16S rDNA sequence of 1258 bp. Phylogenetic analysis using the Mega11 tool validated its classification within the genus Streptomyces. The analysis showed that strain number 173823 originated from a common ancestor (NODE-0) and branched into distinct sub-groups, with notable similarity to strain NRRL2424, indicating high conservation and low evolutionary divergence. The study examined the presence of protein kinase inhibitors (PKIs) in crude extracts of Streptomyces fragilis grown on various media, using *Streptomyces 85E* as a model organism. Inhibition zones were observed in media M:2, M:3, and M:4 for both aqueous and organic extracts, while media M:1 showed no effect. The free radical scavenging assays demonstrated that the

organic extract exhibited superior free radical scavenging capacity with an IC_{50} of 38.76 ± 0.39 µg/mL, compared to the aqueous extract, which had an IC_{50} of 70.68 ± 0.37 µg/mL. However, neither extract matched the potency of the standard drug ascorbic acid, which had an IC_{50} of 14.38 ± 0.14 µg/mL. Protein kinase and antioxidant assays confirmed the superior efficacy of the organic extract, prompting further experiments with it. The cytotoxicity potential of organic crude extracts of Streptomyces fragilis was evaluated against various cell lines (MCF-7, SiHa, PC-3, and Hop-62) through an MTT assay. The extract showed the most substantial inhibitory effect against the MCF-7 (IC_{50} of 61.14 ± 2.5 µg/mL) and SiHa (IC_{50} of 58.46 ± 2.0 µg/mL) cell lines. These findings suggest the further exploration of organic extract to identify and isolate its active compounds and understand their anticancer potential. HR-LCMS analysis of the fermented broth culture revealed a diverse array of bioactive compounds produced by *Streptomyces fragilis*. Computational techniques, including molecular docking, molecular dynamics simulation, and MM/GBSA calculations, were employed to assess the inhibitory activity of these compounds against various kinase proteins. Among the identified compounds, epirubicin demonstrated superior inhibitory activity against key kinase proteins such as CDK4, EGFR, PDGFR, and PI3K when compared to the FDA-approved drug doxorubicin. These findings underscore the significant therapeutic potential of *Streptomyces fragilis*, suggesting it could be a valuable source for the development of novel anticancer agents. In the subsequent chapter, the optimization process was proceeded to enhance the production of secondary metabolites from *Streptomyces fragilis.* By adjusting various parameters and employing advanced computational techniques (RSM and ML), the focus was made to enhance the efficiency and scalability of the production process. Additionally, isolation and characterization of anthracycline or epirubicin from the *Streptomyces fragilis* broth culture were also conducted.